This document is the accepted manuscript version of the following article: Surendra B. Anantharaman, Thilo Stöferle, Frank A. Nüesch, Rainer F. Mahrt,*and Jakob Heier*, Exciton dynamics and effects of structural order in morphology-controlled J-aggregate assemblies, *Adv. Funct. Mater.* **2018,** 1806997; DOI:10.1002/adfm.201806997

DOI: 10.1002/ ((please add manuscript number))
Article type: Full Paper

Exciton dynamics and effects of structural order in morphology-controlled J-aggregate assemblies

Surendra B. Anantharaman, Thilo Stöferle, Frank A. Nüesch, Rainer F. Mahrt, and Jakob Heier**

S. B. Anantharaman, Prof. F. A. Nüesch, Dr. J. Heier
Laboratory for Functional Polymers, Empa, Swiss Federal Laboratories for Materials Science and Technology, Überlandstrasse 129, CH-8600 Dübendorf, Switzerland
E-mail: jakob.heier@empa.ch

S. B. Anantharaman, Prof. F. A. Nüesch
Institut des Matériaux, École Polytechnique Fédérale de Lausanne, EPFL Station 12, CH-1015 Lausanne, Switzerland

Dr. T. Stöferle, Dr. R. F. Mahrt
IBM Research - Zurich, Säumerstrasse 4, CH-8803 Rüschlikon, Switzerland
E-mail: RFM@zurich.ibm.com

Keywords: j-aggregates, narrow-band emitters, morphology, energetic disorder, exciton-quenching

Narrow-band photoluminescence (PL) together with high quantum efficiency from organic molecules is essential for high color purity emitters. Supramolecular assemblies like J-aggregates are promising materials due to their narrow PL signal with full-width at half maximum (FWHM) < 20 nm. However, their micro-crystalline nature and coherent exciton migration results in strong non-radiative exciton recombination at the grain boundaries that diminish the photoluminescence quantum yield (PLQY), and possibilities for improving the crystallinity by tuning the growth mechanism were limited. Here, we demonstrate two distinct routes to grow different J-aggregate morphologies like platelets and lamellar crystals with

improved crystallinity by surface-guided molecular assembly thereby suppressing non-radiative decay and improving PLQY. Both platelets and lamellar crystals show similar absorbance at room temperature. However, temperature-dependent photoluminescence studies show seven-fold (two-fold) higher PLQY for lamellar films compared to platelets at 6 K (300 K). Using time-resolved photoluminescence spectroscopy, different non-radiative decay pathways were identified. The dependence of exciton diffusion on energetic disorder and non-radiative decay will be discussed. The results suggest that the difference in domain size and order gives rise to significantly enhanced radiative decay from lamellar films as compared to platelets or films formed by spin-coating.

1. Introduction

Supramolecular assemblies have attracted immense interest for adding new functionalities to materials. They are widely explored as energy harvesters,[1-3] sensors,[4] plasmonic antennas,[5] polariton lasers,[6] and to build emergent devices like nano-scale exciton-mechanical systems (NEXMS),[7] optical and excitonic switches.[8] Understanding the supramolecular chemistry and the resulting structure–property relation paves the way to bridge the gap from molecular assemblies at the nano-scale to opto-electronic devices at the micron-scale. In particular, packing these molecules one-dimensionally (1D) and two-dimensionally (2D) has revealed unique exciton migration properties, one of the important factors for energy harvesting.[9] Exciton migration distances in amorphous systems of individual monomers are typically on the order of 10 to 20 nm at room temperature, only. Interestingly, self-assembling organic molecules by non-covalent forces can result in strong coupling of the individual transition dipole moments, leading to giant excited state dipoles as observed in J-aggregates.[10-12] These 1D J-aggregates have shown an unprecedented exciton migration up to 1 μm due to low static and energetic disorder.[13-14] Although some 1D aggregates are regarded as the rolled-up form of 2D aggregates, the exciton dynamics in the latter is still ambiguous. For instance, exciton

transport reported from 2D assemblies is only 60 nm, which is well within the individual domain size (~100 nm) of the crystal (~1 μm).[15-16] As self-assembly is known to be a spontaneous organization process, its 2D control on a solid substrate is highly challenging.[17] This spontaneity in self-assembly dictates the crystal size, grain boundaries and energetic disorder which hamper exciton migration.[18-19] Reducing the energetic disorder in the J-aggregates can improve the nature of exciton transport from hopping to band-like transport. Besides exciton migration, 2D assemblies show narrowband emission enabling applications in near-monochromatic, high color purity displays.[18] However, in large area devices, stacking defects in fluorescent 2D assemblies lead to self-quenching, rendering the growth of such structures with high quantum yield very challenging.[2] Finally, growing 2D assemblies on a solid substrate in an aqueous medium is equally demanding for solution-processed printing to fabricate large-area devices. Therefore, it is still necessary to develop an aqueous solution route to grow 2D assemblies on a solid substrate with large crystalline domains thereby enhancing the fluorescence quantum yield for excitonic devices and organic displays.

The focus of the present study, is to demonstrate the growth of different J-aggregates morphologies on functionalized glass substrates. The key control parameters and growth mechanism to obtain high-quality J-aggregate crystals with large coherent domains (3 μm) will be discussed. Furthermore, the influence of the microscopic environment (like grain boundaries, disorder) of the different morphologies on exciton dynamics and fluorescence quenching at low temperature (6 K) will be investigated.

2. Results and Discussion

2.1 Growth mechanism of J-aggregates with different morphologies in solid-state films

We used a solution-processing route to deposit the anionic cyanine dye - TDBC (5,6-dichloro-2-[[5,6-dichloro-1-ethyl-3-(4-sulfobutyl)-benzimidazol-2-ylidene]-propenyl]-1-ethyl-3-(4-sulfobutyl)-benzimidazolium hydroxide, inner salt, sodium salt) on functionalized substrates

to unravel the growth mechanism of 2D J-aggregates and their optical properties. The chemical structure of the TDBC dye is shown in **Figure 1a**. In the first system, TDBC was dissolved in water (c = 0.2 × 10^{-3} M) to form J-aggregates in the solution. The molar extinction coefficient and FWHM of the J-aggregate peak at a wavelength of 587 nm in the solution were determined to be 2.071 × 10^{5} cm^{-1} and ~16 nm (479 cm^{-1}), respectively, by means of steady-state absorption spectroscopy. The peak-fitting for J-aggregate attenuance is shown in Figure S1. Figure 1b shows a schematic of the growth mechanism of J-aggregates from three different dye solutions containing J-aggregates (solution 1), monomers (solution 2) as major phase and mixed monomer and J-aggregate phase (solution 3). The stable phase content in the solution has been achieved by tuning the dye content and solvent mixture, as confirmed from the attenuance in Figure 1(c). Cleaned glass substrates were treated with oxygen plasma and immersed in methanolic polyamidoamine (PAMAM) dendrimer solution (c = 1.0 × 10^{-6} M) and soaked overnight to functionalize the surface. Subsequently, the PAMAM substrates were protonated and immersed in the dye solution to transfer the J-aggregates onto the substrate.[20] The J-aggregates deposited on the PAMAM monolayer substrates were rinsed with Millipore water to remove loosely adsorbed J-aggregate layers. Increasing the PAMAM concentration leads to self-aggregation instead of monolayer formation (Figure S2a and S2b, Supporting Information). Consequently, this resulted in poor J-aggregate formation (irrespective of the solution phase) on the PAMAM substrates, as confirmed by the decrease in J-aggregate absorption (Figure S2c, Supporting Information).

By increasing the immersion time of PAMAM substrates in dye solution (c = 0.2 × 10^{-3} M, solution 1) to 12 h, the deposited J-aggregates formed a *platelets-like* morphology following a 'Volmer-Weber (V-W)' growth model (Figure 1d). The platelets obtained from this growth show numerous small domains isolated by grain boundaries. The V-W growth model is a typical model reported for J-aggregates adsorbed from solution onto AgBr

substrates devoid of any J-aggregate monolayer[21], and is distinctly different from the Stranski-Krastanov (S-K) growth model reported for the same dye, too.[22]

In the second system, the dye solution (c = 0.2 × 10^{-3} M, solution 2) with an equi-volume ratio mixture of methanol:water (50:50) contains monomers as major phase and J-aggregates in a "critical nucleus state". This configuration resulted in selective nucleation of J-aggregates on the PAMAM surface followed by J-aggregate monolayer formation after 12 h. With prolonged time (48 h), the amphiphilic nature of the dye molecule triggered the growth of quasi-epitaxial crystals on top of the J-aggregate monolayer, conforming to a 'S-K' growth model (Figure 1e). The S-K growth process can be explained by the growth of a charged layer on top of the first monolayer of the molecules, complying with charge neutrality. Our findings suggest that templated molecular assembly is a highly efficient process to realize different solid-state J-aggregate morphologies like platelets, monolayers, and quasi-epitaxial crystals. To confirm the difference in thin film molecular packing between platelets and quasi-epitaxial crystals, we have investigated their crystalline nature using small-angle x-ray scattering (SAXS) using a synchrotron source. From the SAXS data (Figure S3), we can confirm that molecules are randomly oriented in platelets, signifying polycrystallinity, whereas they are uni-directionally oriented for quasi-epitaxial crystals. It should be noted that the x-ray diffraction intensity is very significant from a thin film (~10 nm, "platelets"), and the absence of diffraction peaks in quasi-epitaxial crystals (~150 nm) is not due to a reduced scattering volume.

Based on these observations, we have developed a new strategy to grow J-aggregate crystals of the TDBC dye with reduced grain boundaries on the PAMAM substrate. This is achieved by adjusting the ratio of monomers and J-aggregates in an equi-volume ratio solution of methanol and water (c = 0.8 × 10^{-3} M, solution 3) such that J-aggregates anchor on the substrate, and monomers are fed from the solution to grow high quality crystals. The morphology obtained from this new route is subsequently referred to as *lamellar* films (Figure

1f). It is evident from the scanning force microscopy images that the crystalline domains in the lamellar film are significantly larger (~ 3 μm) compared to the platelets (~ 30–50 nm). Histograms of height and domain size for platelets and lamellar films are shown in Figure S4 (Supporting Information). For comparison with the V-W route, as shown in Figure 1(d), we have deposited J-aggregates from a high dye concentration (0.8×10^{-3} M) in water for 12 h, which did not lead to larger aggregate domains. This confirms that the controlled growth of aggregates from a dye solution containing J-aggregates supplemented by free monomers is key to form high quality lamellar crystals in the solid-state. This condition is achieved by employing a methanol-water co-solvent system with high dye concentration.

Following the discussion above, it turns out that at low dye concentration (0.2 mM, 0.175 mg/ml) with J-aggregates as major phase in the water solution, platelets (leaves-like) are the only morphology obtained. However, keeping the same dye concentration (0.2 mM, 0.175 mg/ml) with monomers as major phase and J-aggregates in critical nucleus 50:50 methanol:water solution, quasi-epitaxial crystals (stripes) were observed. Upon increasing the dye concentration (0.8 mM, 0.7 mg/ml) in the binary solvent mixture containing both monomers and J-aggregates leads to a mixed morphology of leaf-like morphology and stripes in lamellar films. This concours with the morphological arrangements for a similar carbocyanine dye molecule reported by Prokhorov *et.al.*[23], where high dye concentration (0.5 mg/ml) has led to the formation of both leaves and stripe J-aggregate morphology. Note that the dye concentration used in this work to obtain lamellar films is close to the concentration reported by Prokhorov *et.al.*[23] Here, we demonstrate that tuning the dye concentration to control the monomer and J-aggregate content in solution allows obtaining distinct morphologies in thin films.

2.2 Optical properties of platelet and lamellar films

Optical properties of monomers in solution and J-aggregate films of platelets and lamellar structures are compared in **Figure 2**a. The monomer dye solution exhibits an absorption peak around 518 nm followed by vibronic progression and its corresponding photoluminescence (PL) peak at 541 nm, with a large spectral shift of about 23 nm (821 cm^{-1}). Upon formation of J-aggregates, the transition dipole moments of the monomer molecules are strongly coupled, leading to a red-shifted narrow absorption band peaked at 587 nm with a FWHM of ~13 nm (393 cm^{-1}). Although lamellar films showed higher attenuance than platelets, the absorbance of the films measured in an integrating sphere was almost the same. This points towards stronger light scattering of the lamellar films compared to the platelet's films, as expected from the much larger domain size. In addition, the PL signals of the J-aggregate films were recorded in an integrating sphere at room temperature. Despite the presence of J-aggregate monolayers in lamellar films that can cause strong reabsorption, lamellar films showed more intense PL than the platelets when comparing the spectrally integrated PL intensity. The absolute quantum yield values obtained for platelets and lamellar films following deMello's[24] method and PL spectrum corrected for reabsorption[25] are 2.34% and 4.59%, respectively. The true absorbance for both films at the excitation wavelength (550 nm) was similar (0.04). Furthermore, as an external reference standard, the absolute PLQY for Rhodamine 101 dye solution was measured as reported by Würth *et.al.*[26], showing only little deviation (86% instead of 91 % as reported by Würth *et. al.*[26]). The spectral shift for both J-aggregate films is only ~5 nm (144 cm^{-1}). Small spectral shift, narrow PL signal and higher PLQY suggest that the lamellar films could be more promising than platelets regarding energy transport properties.

Deeper insight into the exciton dynamics is gained by investigating the fluence dependence of the PL at various temperatures ranging from 6 K up to 100 K for both platelets and lamellar films. A pulsed laser with an excitation wavelength of 400 nm, 80 MHz repetition rate, 100 fs pulse duration, and incident fluence of up to 100 nJ cm^{-2} was used for

excitation. The exciton density is very low within this range, safely ruling out singlet-singlet exciton annihilation.[13, 15] At 6 K, the relative quantum yield of lamellar films was almost seven-fold higher compared to platelets (Figure 2b). Moreover, the FWHM of the PL signal was much narrower for the lamellar films, pointing towards a larger coherent domain size and an enhanced PLQY.[18] It should be noted that no long-wavelength components were observed unlike in 1D aggregates, which are reported to be exciton traps.[27] From 6 K to 100 K (Figure 2b) and even at room temperature (Figure 2a) the relative quantum yield of the lamellar films remained higher compared to platelet films, suggesting that less non-radiative decay channels are present. Furthermore, the PL intensity did not follow a linear decrease with temperature, in good agreement with a recent report.[19]

2.3 Exciton dynamics in platelets and lamellar films at low temperature (6 K)

Figure 3a summarizes the PL intensity *versus* excitation fluence recorded at 6 K. Power-law fits to the emitted intensity allowed to identify density-dependent quenching mechanisms for the different morphologies and excess photon energies resulting in a sub-linear behavior (exponent <1). Upon exciting with a pulsed laser at 550 nm (80 MHz, 100 fs pulse duration) a linear increase (PL α $I^{1.0\ (0.94\pm0.05)}$) in PL intensity with increasing pump fluence I for lamellar (platelet) films was observed. However, exciting with high energy photons (400 nm, 80 MHz repetition rate, 100 fs pulse duration) a pronounced sub-linear behavior in platelets (PL α $I^{0.77\pm0.05}$) compared to the lamellar (PL α $I^{0.94\pm0.05}$) films has been observed. Continuous-wave (CW) excitation at 405 nm shows similar sub-linear behavior (PL α $I^{0.86\pm0.05}$) for both films. Due to the very low excitation densities, the observed sub-linear behavior cannot be attributed to exciton-exciton annihilation (EEA), as observed in experiments with high excitation fluence.[13, 15] Hence, we consider the sub-linear behavior to be an indirect consequence of the excess energy of the optical excitation, which will be discussed below.

By means of time-resolved PL spectroscopy, the exciton dynamics was investigated for platelets, lamellar and spin-coated films with 400 nm pulsed laser excitation at 6 K, as shown in Figure 3b. The temporal PL decay was fitted by a mono-exponential, and alternatively, a bi-exponential function. The fitting parameters are summarized in Table 1. The goodness of fit (G.O.F) does not significantly improve by using a bi-exponential fit compared to a mono-exponential fit, confirming the results reported by Lindrum *et.al.*[28] showing that a mono-exponential fit is the best approximation for the PL decay at low temperature ($T \leq 20$ K) and a bi-exponential fit is applicable for room temperature measurements. Therefore, we used mono-exponential decay fitting in our study, implying that one excited state dictates the exciton dynamics. However, one has to take into account that disorder like a non-uniform distribution of domain sizes typically leads to a non-exponential decay behavior. Lamellar films showed faster decay dynamics compared to platelets and spin-coated films. This observation in conjunction with the higher PLQY suggests that larger coherent domains are present in the lamellar film.[29] By increasing the fluence, the PL intensity increased, concomitant with a slight decrease in the lifetime (Table S2, Supporting Information). In addition, lifetime measurements for lower excitation fluence of 26 nJ cm^{-2} are shown in Figure S7, Supporting Information.

The polydispersity of the crystalline domains of the platelets or spin-coated films, due to the presence of intra-granular sub-structures[30] (see Figure 1b), results in an inhomogeneously broadened density of states (DOS), similar to observations in ensembles of perovskite nanocrystals and colloidal quantum dots.[31-32] Excitons in the vicinity of inter-grain boundaries will be immediately quenched non-radiatively and therefore decrease the PLQY.[33-34] On the other hand, monodispersity and less topological disorder in lamellar films are accompanied by comparatively less energetic disorder. Direct evidence of energetic disorder can be drawn from the streak camera images (Figure 3c, d), and spectra taken at

different times (cross-sections from the images), showing a slightly more pronounced red-shift that increased with time more for platelets compared to lamellar films (Figure 3e).

From the experimental results described above, the following conclusion can be drawn: the sub-linear power-dependence and the dependence on the excess energy of the pump photons suggest that the observed PL behavior stems from a charge generation mechanism resulting in non-radiative quenching of excitons. The generation of charges depends on the excitation photon energy as well as on the excitation laser fluence. An excitation generated in a localized state subsequently executes a random walk within a manifold of positionally and energetically disordered sites towards the tail states of the DOS because under non-equilibrium conditions and at low temperatures (6 K) downward jumps in energy dominate the random walk. This behavior is schematically shown in **Figure 4**a and b. Exciting the films at 505 nm, 1 kHz repetition rate (2.45 eV) with an excess energy of only ~200 meV relative to the S_1-S_0 transition, and taking into account that the laser fluence in this experiment was significantly higher (Table S2) leading to higher exciton densities and possibly to additional quenching mechanisms, still a substantially longer exciton lifetime was observed compared to excitation at 400 nm (80 MHz repetition rate) with an excess energy of ~850 meV (see Table S2). This signifies that the excess energy for excitation at 505 nm is insufficient to generate free charges, and therefore grain boundaries and/or other permanent non-radiative traps like H-type aggregates are the dominating exciton quenching sites.[35] The observed increase in lifetime with excitation density could indicate that these traps are gradually filled. Lifetime measurements with low-fluence pulses at 550 nm and 80 MHz repetition could not be done due to technical constraints in the setup. However, excitation at 400 nm led to the creation of free charges as observed also in conjugated polymers[36-39] and aggregates[40] (Figure 4c and d). Here, the excess energy created a vibrationally hot excitation (bound electron-hole pair) which can subsequently dissociate. Once separated, the carriers have a reduced probability to recombine again, leading to free charge carriers.[36, 41] The

calculations for the charge recombination time and the diffusion length are detailed in the Supporting Information. The lifetime of the free charges (15 μs) is much longer than the exciton lifetime (~10 ps) which results in exciton-charge quenching. Furthermore, as seen in Figure 3a, such exciton-charge quenching is independent of the excitation mode (CW (405 nm) and pulsed laser (400 nm)) which leads to sub-linear behavior.

Owing to low mobility of the free charge carriers at low temperatures, the charges are trapped in the immediate vicinity of defects. This residing charge species form a *trap state* preferentially at the grain boundaries, quenching the excitons.[34] Such additional non-radiative process explains both the sub-linearity and the lower QY in platelets compared to lamellar films. Consequently, lamellar films with a comparably low number of granular boundaries result in higher PLQY. In addition, spin coated films (topography is shown in Figure S8) were investigated under similar conditions with power-dependent PL measurements, yielding a power-law exponent of 0.19. Hence, photo-induced charge generation efficiency increased with disorder in the film, thus confirming this model. It should be noted that by increasing the defect concentration (grain boundaries) from lamellar films to platelets to spin-coated films, the lifetime increased and the power-law exponent of the power-dependent PL intensity was more pronounced sub-linear (0.94 to 0.19). This cannot be consistently explained from the coherent domain size and exciton lifetime alone and may be due to additional defects introduced in the film during processing that can lead to further charge generation and luminescence quenching. For instance, matrix immobilization of J-aggregates has shown Lévy (non-Gaussian) type of disorder in the films.[42] Such Lévy-type of defects are reported to significantly funnel excitons to trap states present in the film.[43] On the other hand, such disorder can also induce exciton self-trapping.[44]

We note that both the almost linear PL intensity as a function of excitation fluence in lamellar films as well as the sub-linear behavior in platelets remained constant (in the error range for the exponent of ±0.05) within the temperature range of the measurements (Figure

S9, Supporting Information). This suggests a temperature-independent charge generation and trapping rate and a minor role of temperature-driven exciton or charge diffusion for this kind of quenching process. The larger energetic disorder in platelets leads to increased charge generation, and consequently, to stronger exciton quenching compared to lamellar films, resulting in stronger sub-linearity in the former. In contrast, the lower energetic disorder in lamellar films can inhibit photocarrier generation, and therefore circumvent exciton quenching, allowing for enhanced exciton diffusion. Our observations manifest the interplay of topological and energetic disorder, which can strongly dictate exciton dynamics in the absence of exciton-phonon interaction.

3. Conclusion

In summary, two different routes to form molecular assemblies of cyanine dyes on solid substrates following two different growth models were introduced. The presence of critical J-aggregate nuclei is pivotal to switch its growth mode on solid substrates. Using different excitation schemes (CW, pulsed, varying the excess energy) as well as time-resolved PL spectroscopy, different non-radiative decay pathways were identified. The interplay of energetic disorder and non-radiative decay are dominant factors affecting the exciton transport. The results show that the difference in domain size and order give rise to significantly enhanced radiative decay for lamellar films as compared to platelets or films deposited by spin-coating. This growth methodology can be employed to design crystalline and highly fluorescent 2D materials which will have potential for future opto-electronic devices.

4. Experimental Section

Growth of J-aggregate films: PAMAM dendrimers (10 wt% in methanol, Sigma Aldrich) with ethylene diamine core, generation 4.0 solution was used for functionalizing the glass substrates. The anionic cyanine dye 5,6-dichloro-2-[[5,6-dichloro-1-ethyl-3-(4-sulfobutyl)-

benzimidazol-2-ylidene]-propenyl]-1-ethyl-3-(4-sulfobutyl)-benzimidazolium hydroxide, inner salt, sodium salt (TDBC) was purchased from FEW chemicals, Germany and used without any further purification. TDBC was dissolved in water (Millipore water, 18.2 MΩ·cm resistivity at 25 °C) and in methanol-water (50:50) mixture, separately with a dye concentration (*c*) of 0.2×10^{-3} M (0.175 mg/ml), to study the self-assembly of dyes towards formation of J-aggregates on functionalized surface. Also, a high dye concentration ($c = 0.8 \times 10^{-3}$ M) solution was prepared by dissolving 0.7 mg/ml in methanol-water (50:50) mixture. 5 mg of dye was dissolved in 1 ml of water and stirred overnight before spin coating on glass substrates at 4000 rpm for 60 s.

Surface functionalization and film formation: Glass substrates were cleaned following a standard procedure by ultra-sonicating them in 0.2 % Hellmanex solution, water, acetone, ethanol for 10 min individually. Followed by cleaning, glass substrates were treated with oxygen plasma with a power setting of 45 W for 5 min. Plasma-treated glass was immediately immersed in PAMAM ($c = 1\times10^{-6}$ M) methanolic solution for 18 h to functionalize the surface. Such functionalized layer was rinsed with methanol to remove loosely adsorbed PAMAM while leaving behind a monolayer. Subsequently, the PAMAM-coated substrates were protonated in acidic (pH < 3) medium to activate the amine groups for anchoring anionic dye molecules.[20] Protonated PAMAM-coated substrates were immersed in the dye solution for various time schedules with mild shaking and rinsed with Millipore water to obtain J-aggregate films.

Scanning probe microscopy (SPM): SPM studies were conducted using a Bruker Dimension Icon in tapping mode to map the topography and phase contrast of the J-aggregate films. Antimony-doped Si cantilevers (RTESP-300) procured from Bruker with a tip radius of 12 nm, force constant of 40 Nm^{-1} and operating at resonant frequency of 300 kHz were used. The

SPM images were analyzed using the NanoScope software using particle analysis with a threshold height to the maximum of the height histogram to deduce height and domain size histograms.

Grazing incidence small angle x-ray diffraction studies (SAXS): SAXS measurements for the platelets and quasi-epitaxial crystals were performed at the Elettra synchrotron facility (Trieste, Italy). A 1D gas detector (Gabriel type) calibrated with silver behanate for the scattering vector (q) values was used to collect the scattered x-rays from the sample. The sample-to-detector distance was fixed at 176 cm with a fixed wavelength (λ = 1.54 Å). The scattering vector (q) is defined as $q = 4\pi\sin(\theta)/\lambda$, where 2θ is the scattering angle.

Attenuance and steady-state photoluminescence: Attenuance for monomer solution and J-aggregate films were characterized using a Varian Cary 50 UV-Vis spectrophotometer. Absorbance and steady-state photoluminescence spectra of the deposited J-aggregate films and monomer solution were studied using a Horiba Jobin-Yvon Fluorolog spectrofluorometer equipped with an integrating sphere. The absolute quantum yield for the platelet and lamellar films were measured at room temperature using an integrating sphere.[24] Furthermore, as an external standard to evaluate the deviation of quantum yield values as determined from our instrument, we have measured a Rhodamine 101 dye solution using a quartz-cuvette (10 x 10 mm) following the protocol mentioned elsewhere.[26] Due to small Stokes' shift in J-aggregate thin films, the reabsorption of the fluorescence spectrum was corrected by following the approach proposed by Cao and Sletten.[25] Briefly, the true fluorescence ($I(\lambda)$) was obtained by correcting for reabsorption from the overlap between absorption and emission spectra as,

$$I(\lambda) = I_0(\lambda)\left[\frac{-\ln(10^{-OD(\lambda)})}{1-(10^{-OD(\lambda)})}\right] \qquad (0)$$

where, $I_0(\lambda)$ is the experimental value, $OD(\lambda)$ is the optical density of the sample.

Laser fluence studies and time-resolved photoluminescence spectroscopy (TRPL): J-aggregate thin films were mounted in a liquid Helium flow cryostat maintained in Helium exchange gas and cooled to 6 K. Excitation fluence series for the films were acquired by using excitation either at 400 nm by a frequency-doubled mode-locked Ti:Sapphire laser or alternatively at 550 nm by an optical parametric oscillator (OPO) pumped by the mode-locked Ti:Sapphire, with a pulse duration of about 100 fs and a repetition rate of 80 MHz, respectively. For comparison, additional PL experiments by means of a continuous-wave laser with an excitation wavelength at 405 nm have been carried out. A travelling-wave parametric amplifier pumped by a Ti:Sapphire regenerative amplifier (800 nm, 1 kHz) seeded by the Ti:Sapphire laser was used to excite the films at 505 nm with a pulse duration of about 250 fs and 1 kHz repetition rate. Time- and spectrally-resolved PL for excitation at 400 nm (80 MHz) and 505 nm (1 kHz) laser was measured by means of a streak camera (Hamamatsu, nominal time resolution 2 ps) coupled to a spectrometer. Temperature-dependent PL signals were recorded at different temperatures ranging from 6 K to 100 K. The integrated area of the PL signal was normalized to PL from platelet films (as a reference for relative quantum yield) at 6 K. For plotting the full-width at the half-maximum (FWHM) of the PL signal at different temperatures, the PL spectrum at 6 K was fitted using Voigt function to determine the Gaussian ($\Delta\omega_G$) and Lorentzian ($\Delta\omega_L$) width. As Gaussian width represents static energetic disorder (T-independent) and Lorentzian width represents T-dependent perturbations, the value of Gaussian width calculated at 6 K was fixed as constant while applying Voigt fitting for other temperatures up to 100 K. From the Gaussian width and Lorentzian width, the FWHM of the PL signal is calculated as,

$$FWHM = (0.5346 \times \Delta\omega_L) + \sqrt{(0.2169 \times \Delta\omega_L^2) + \Delta\omega_G^2} \qquad (0)$$

For plotting the transient energetic shift, the spectral data points are binned in time intervals of 4 ps. The data points were fitted to a Gaussian profile to determine the peak energy for the transient energetic shift along with the error in the peak energy value from the fitting.

Supporting Information
Supporting Information is available from the Wiley Online Library or from the author.

Acknowledgements

The authors gratefully acknowledge funding from the Swiss National Science Foundation grant number: 200021-157135 to conduct this research work. We acknowledge the Scanning Probe Microscopy user laboratory at Empa for providing access to the instrument. This work was partly supported by the Swiss State Secretariat for Education, Research and Innovation (SERI) and the European Union's Horizon-2020 framework programme through the Marie-Sklodowska Curie ITN network SYNCHRONICS (H2020-MSCA-ITN-643238). We thank Stefan Salentinig, Laboratory for Biointerfaces, Empa St. Gallen for the SAXS measurement and access to the Elettra facility.

Received: ((will be filled in by the editorial staff))
Revised: ((will be filled in by the editorial staff))
Published online: ((will be filled in by the editorial staff))

References

[1] J.-L. Brédas, E. H. Sargent, G. D. Scholes, *Nature Materials* **2016**, 16, 9.
[2] H. Q. Peng, Y. Z. Chen, Y. Zhao, Q. Z. Yang, L. Z. Wu, C. H. Tung, L. P. Zhang, Q. X. Tong, *Angewandte Chemie International Edition* **2012**, 51, 2088.
[3] S. Sengupta, F. Würthner, *Accounts of Chemical Research* **2013**, 46, 2498.
[4] W. Liang, S. He, J. Fang, *Langmuir* **2014**, 30, 805.
[5] A. Cacciola, C. Triolo, O. Di Stefano, A. Genco, M. Mazzeo, R. Saija, S. Patanè, S. Savasta, *ACS Photonics* **2015**, 2, 971.
[6] G. G. Paschos, N. Somaschi, S. I. Tsintzos, D. Coles, J. L. Bricks, Z. Hatzopoulos, D. G. Lidzey, P. G. Lagoudakis, P. G. Savvidis, *Scientific Reports* **2017**, 7, 11377.
[7] P. Deotare, Nanoscale Exciton-Mechanical Systems (NEXMS), http://eecs.umich.edu/eecs/about/articles/2016/parag-deotare-receives-afosr-young-investigator-award.html, accessed: April 2018.
[8] G. Grosso, J. Graves, A. T. Hammack, A. A. High, L. V. Butov, M. Hanson, A. C. Gossard, *Nature Photonics* **2009**, 3, 577.
[9] A. G. Dijkstra, H.-G. Duan, J. Knoester, K. A. Nelson, J. Cao, *The Journal of Chemical Physics* **2016**, 144, 134310.
[10] D. Möbius, H. Kuhn, *Journal of Applied Physics* **1988**, 64, 5138.
[11] D. Möbius, *Advanced Materials* **1995**, 7, 437.
[12] S. Kirstein, H. Möhwald, *Advanced Materials* **1995**, 7, 460.

[13] J. R. Caram, S. Doria, D. M. Eisele, F. S. Freyria, T. S. Sinclair, P. Rebentrost, S. Lloyd, M. G. Bawendi, *Nano Letters* **2016**, 16, 6808.
[14] D. M. Eisele, J. Knoester, S. Kirstein, J. P. Rabe, D. A. Vanden Bout, *Nature Nanotechnology* **2009**, 4, 658.
[15] G. M. Akselrod, Y. R. Tischler, E. R. Young, D. G. Nocera, V. Bulovic, *Physical Review B* **2010**, 82.
[16] S. Valleau, S. K. Saikin, M.-H. Yung, A. A. Guzik, *The Journal of Chemical Physics* **2012**, 137, 034109.
[17] S. L. Cai, W. G. Zhang, R. N. Zuckermann, Z. T. Li, X. Zhao, Y. Liu, *Advanced Materials* **2015**, 27, 5762.
[18] J. Knoester, *Advanced Materials* **1995**, 7, 500.
[19] A. Eisfeld, C. Marquardt, A. Paulheim, M. Sokolowski, *Physical Review Letters* **2017**, 119, 097402.
[20] R. Steiger, R. Pugin, J. Heier, *Colloids and Surfaces B: Biointerfaces* **2009**, 74, 484.
[21] H. Saijo, M. Shiojiri, *Journal of Imaging Science and Technology* **1997**, 41, 266.
[22] M. S. Bradley, J. R. Tischler, V. Bulović, *Advanced Materials* **2005**, 17, 1881.
[23] V. V. Prokhorov, S. I. Pozin, D. A. Lypenko, O. M. Perelygina, E. I. Mal'tsev, A. V. Vannikov, *Chemical Physics Letters* **2012**, 535, 94.
[24] J. C. de Mello, H. F. Wittmann, R. H. Friend, *Advanced Materials* **1997**, 9, 230.
[25] W. Cao, E. M. Sletten, *Journal of the American Chemical Society* **2018**, 140, 2727.
[26] C. Würth, M. Grabolle, J. Pauli, M. Spieles, U. Resch-Genger, *Nature Protocols* **2013**, 8, 1535.
[27] M. Vacha, M. Furuki, T. Tani, *The Journal of Physical Chemistry B* **1998**, 102, 1916.
[28] M. Lindrum, A. Glismann, J. Moll, S. Daehne, *Chemical Physics* **1993**, 178, 423.
[29] F. C. Spano, J. R. Kuklinski, S. Mukamel, D. V. Brumbaugh, M. Burberry, A. A. Muenter, *Molecular Crystals and Liquid Crystals* **1991**, 194, 331.
[30] H. Asanuma, T. Tani, *The Journal of Physical Chemistry B* **1997**, 101, 2149.
[31] H.-H. Fang, L. Protesescu, D. M. Balazs, S. Adjokatse, M. V. Kovalenko, M. A. Loi, *Small* **2017**, 13, 1700673.
[32] G. M. Akselrod, F. Prins, L. V. Poulikakos, E. M. Y. Lee, M. C. Weidman, A. J. Mork, A. P. Willard, V. Bulović, W. A. Tisdale, *Nano Letters* **2014**, 14, 3556.
[33] R. R. Lunt, J. B. Benziger, S. R. Forrest, *Advanced Materials* **2010**, 22, 1233.
[34] J. D. A. Lin, O. V. Mikhnenko, T. S. van der Poll, G. C. Bazan, T.-Q. Nguyen, *Advanced Materials* **2015**, 27, 2528.
[35] O. P. Dimitriev, Y. P. Piryatinski, Y. L. Slominskii, *The Journal of Physical Chemistry Letters* **2018**, 9, 2138.
[36] V. I. Arkhipov, E. V. Emelianova, H. Bässler, *Physical Review Letters* **1999**, 82, 1321.
[37] C. Deibel, D. Mack, J. Gorenflot, A. Schöll, S. Krause, F. Reinert, D. Rauh, V. Dyakonov, *Physical Review B* **2010**, 81, 085202.
[38] D. J. Carswell, L. E. Lyons, *Journal of the Chemical Society (Resumed)* **1955**, DOI: 10.1039/JR95500017341734.
[39] E. Hendry, M. Koeberg, J. M. Schins, H. K. Nienhuys, V. Sundström, L. D. A. Siebbeles, M. Bonn, *Physical Review B* **2005**, 71, 125201.
[40] Z. Guo, D. Lee, H. Gao, L. Huang, *The Journal of Physical Chemistry B* **2015**, 119, 7666.
[41] D. M. Basko, E. M. Conwell, *Physical Review B* **2002**, 66, 155210.
[42] L. Lüer, S. K. Rajendran, T. Stoll, L. Ganzer, J. Rehault, D. M. Coles, D. Lidzey, T. Virgili, G. Cerullo, *The Journal of Physical Chemistry Letters* **2017**, DOI: 10.1021/acs.jpclett.6b02704547.
[43] A. Merdasa, Á. J. Jiménez, R. Camacho, M. Meyer, F. Würthner, I. G. Scheblykin, *Nano Letters* **2014**, 14, 6774.

[44] A. V. Sorokin, N. V. Pereverzev, I. I. Grankina, S. L. Yefimova, Y. V. Malyukin, *The Journal of Physical Chemistry C* **2015**, 119, 27865.

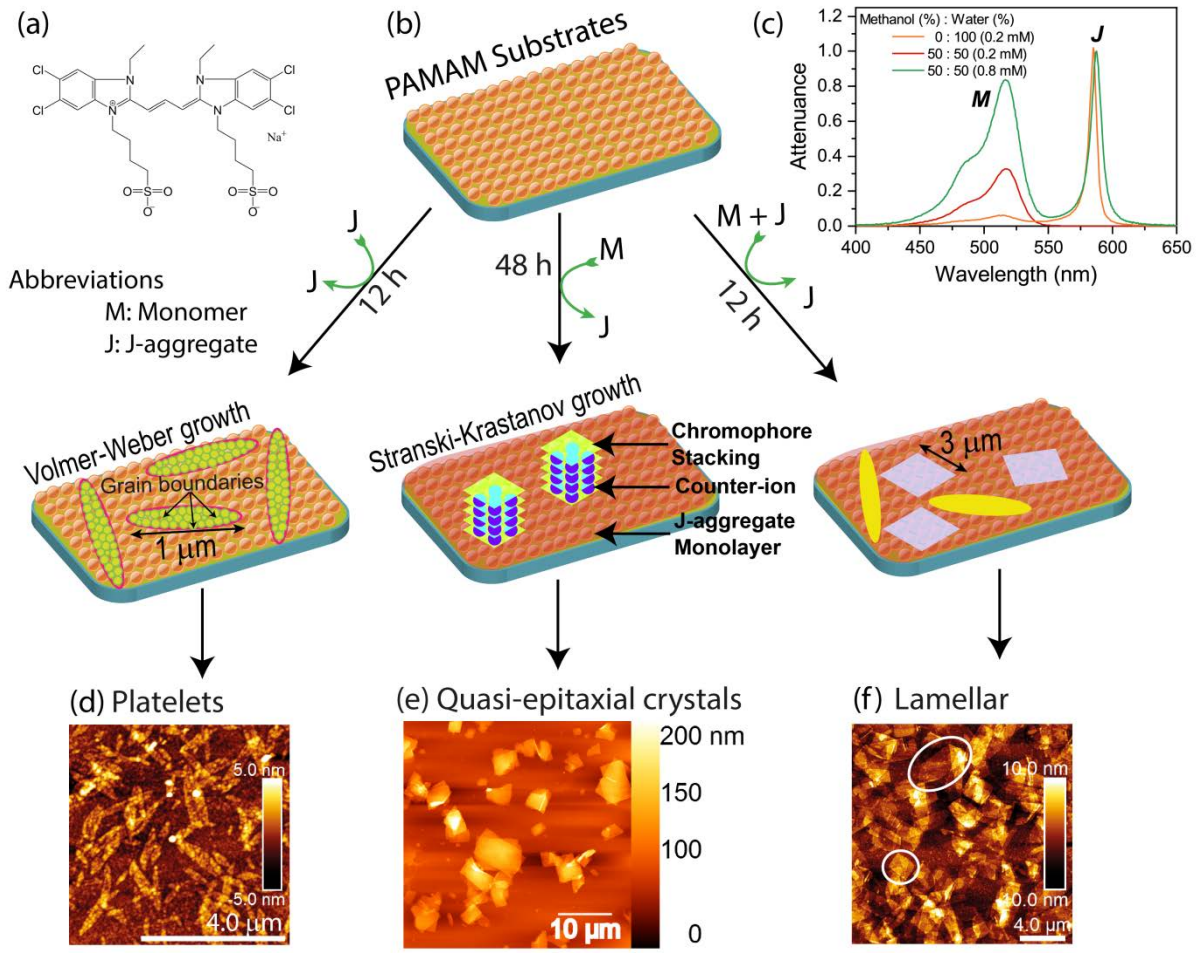

Figure 1. (a) Chemical structure of the TDBC dye. (b) Schematic showing methodologies to control J-aggregates growth following Volmer-Weber and Stranski-Krastanov growth models. (c) Attenuance of dye solution by varying the monomer and J-aggregate phase content leads to different types of J-aggregate morphologies like (d) platelets, (e) quasi-epitaxial crystals and (f) lamellar on glass substrates functionalized with PAMAM, as observed with scanning probe microscopy. Presence of mixed leaf-like and stripe J-aggregates in lamellar films are marked with white rings in (f).

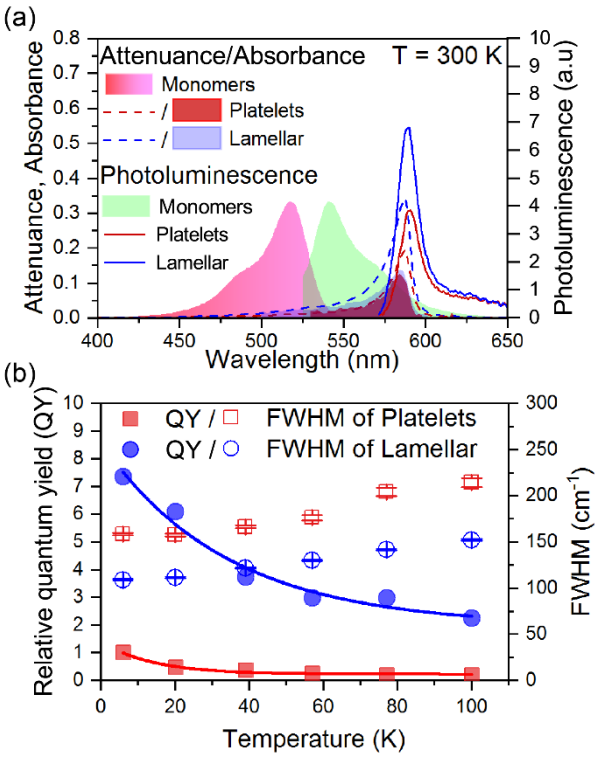

Figure 2. (a) Attenuance, absorbance and steady-state photoluminescence of monomers in methanolic solution, platelets and lamellar film measured at 300 K. Photoluminescence signals of the thin films are recorded with an excitation wavelength of 530 nm (450 nm for monomers) in an integrating sphere. Attenuance at 300 K and PL at 6 K and 300 K are shown in the SI. (b) Relative quantum yield for the platelets and lamellar films from 6 to 100 K, normalized to the quantum yield of platelets films at 6 K, with pulsed excitation wavelength at 400 nm and 80 MHz repetition rate. The corresponding full-width at half-maximum (FWHM) of the photoluminescence of the thin films, as shown in Table S1, are plotted as a function of temperature. The error bars from the fit are smaller than the symbol size.

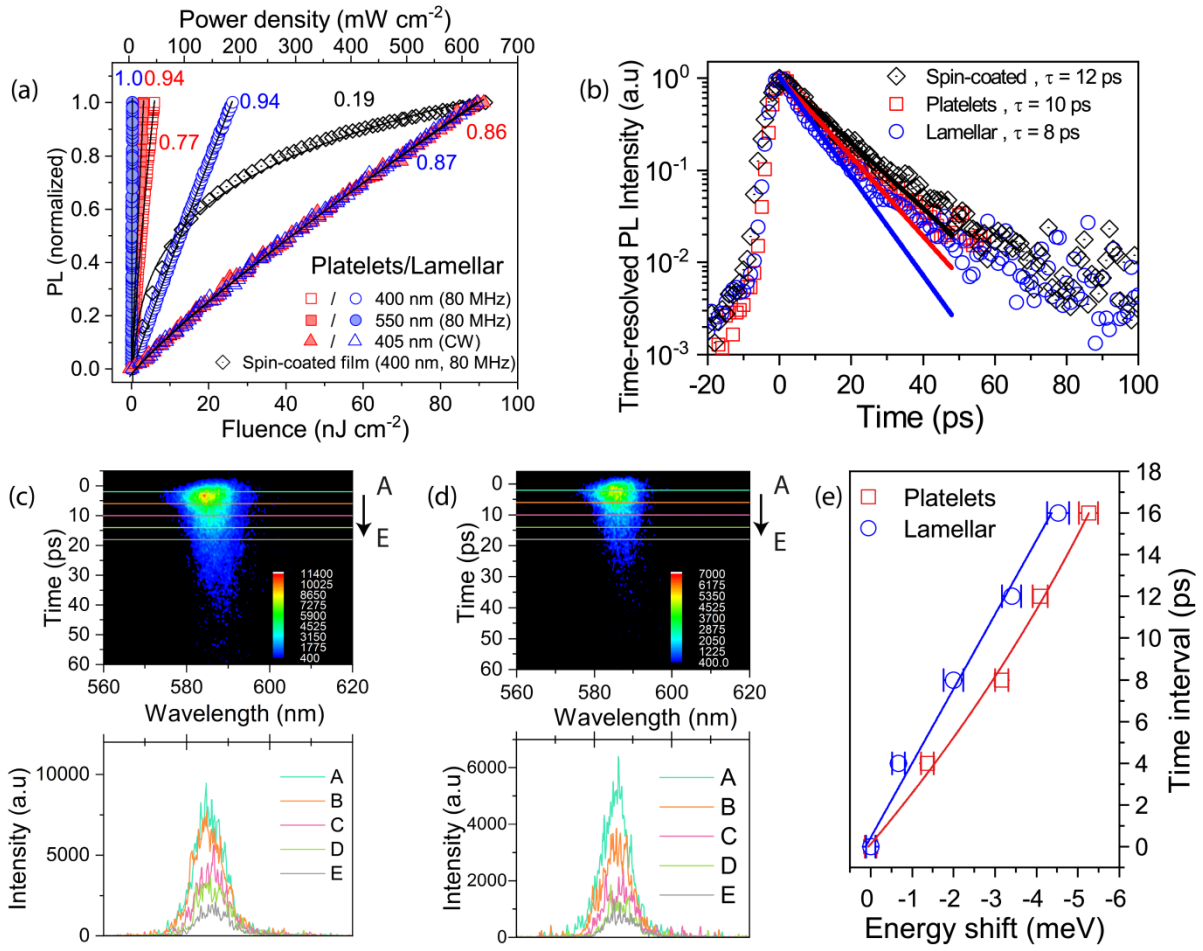

Figure 3. (a) Spectrally- and temporally-integrated photoluminescence acquired with continuous-wave and ultrafast excitation at 400 nm and 550 nm for platelets and lamellar films at 6 K. For comparison, spin coated films were studied with ultrafast excitation at 400 nm, 80 MHz at 6 K. The exponents from the power-law fits (PL α I^n) are added as labels to the curves (See Figure S5, SI for unnormalized raw data). For reversibility, see Figure S6, SI. The top horizontal axis represents the power density range used for the CW excitation. (b) Time-resolved spectrally-integrated dynamics (fluence of 78 nJ cm^{-2}) with the lines representing the fits of an exponential decay to the data between 0 and 50 ps. From this, the exciton lifetime for the films was extracted (mono exponential decay times are shown in the legend). Cross-sections plotted for small time intervals (4 ps bin size) from the streak camera image recorded with an excitation wavelength of 400 nm for platelets (c) and lamellar films

(d). (e) Transient red-shift in peak center energies from (c) and (d) with error bars for the peak energies corresponding to the time. Lines are a guide to the eye.

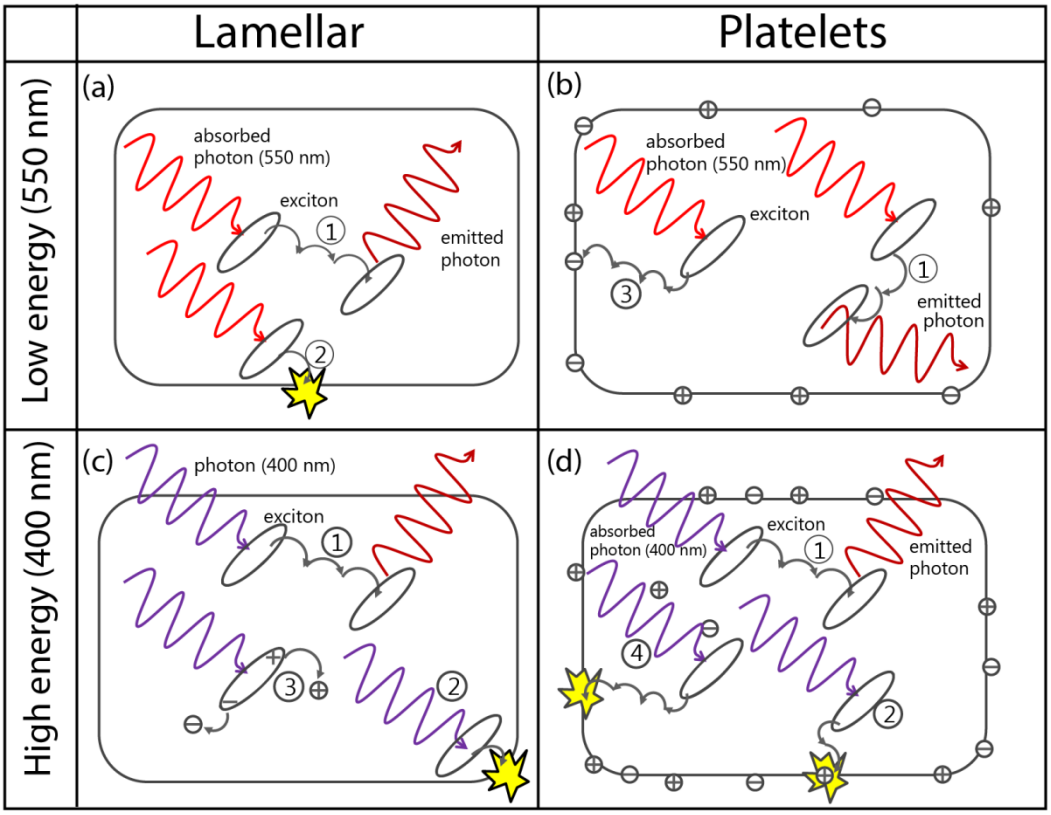

Figure 4. Schematic representation of exciton dynamics in lamellar (a) and platelet (b) films when excited at 550 nm. In comparison, charge generation in the bulk films for lamellar (c) and platelets (d) leads to exciton quenching when excited at 400 nm. ① - exciton diffusion and radiative recombination, ② - non-radiative recombination at disordered sites, ③ - charge-carrier generation and ④ - exciton-charge quenching in the bulk along with ② .

Table1. Exciton lifetime values obtained from mono-exponential and bi-exponential decay fits.

Sample	Mono-exponential fit			Bi-exponential fit					
	Amplitude (A)	Lifetime (τ), in ps	G.O.F[#]	Amplitude (A_1)	Lifetime (τ_1), in ps	Amplitude (A_2)	Lifetime (τ_2), in ps	G.O.F[#]	A_1/A_2
Lamellar	1.03±0.01	8	0.9895	0.94±0.03	6	0.12±0.03	26	0.9958	7.83
Platelets	1.02±0.01	10	0.9887	0.88±0.08	6	0.29±0.09	18	0.9970	3.03
Spin-coated films	1.02±0.01	12	0.99188	0.93±0.06	10	0.10±0.06	34	0.9954	9.3

[#]-goodness of fit

Narrow-band photoluminescence (PL) from supramolecular assemblies is non-radiatively quenched by grain boundary annihilation. Here we show that excess energy through optical excitation can foster exciton dissociation. Exciton-charge quenching is then an additional non-radiative decay channel which decreases the PL. Growing high quality crystals and reducing the number of grain boundaries can obviate non-radiative quenching processes to significantly enhance the PL.

Keywords: j-aggregates, narrow-band emitters, morphology, energetic disorder, exciton-quenching

Surendra B. Anantharaman, Thilo Stöferle, Frank A. Nüesch, Rainer F. Mahrt,* and Jakob Heier*

Exciton dynamics and effects of structural order in morphology-controlled J-aggregate assemblies

ToC figure